ISSN 1069-3513, Izvestiya, Physics of the Solid Earth, 2018, Vol. 54, No. 3, pp. 466–473. © Pleiades Publishing, Ltd., 2018.
Original Russian Text © M.V. Abakumov, V.M. Chechetkin, S.L. Shalimov, 2018, published in Fizika Zemli, 2018, No. 3.

Mathematical Simulation of Convective Processes in the Liquid Core of the Earth and Implications for the Interpretation of Geomagnetic Field Variations in Polar Latitudes

M. V. Abakumov[a, *], V. M. Chechetkin[b, c, **], and S. L. Shalimov[d, *]**

[a] *Moscow Faculty of Computational Mathematics and Cybernetics, Moscow State University, Moscow, 119991 Russia*
[b] *Keldysh Institute of Applied Mathematics, Russian Academy of Science, Moscow, 125047 Russia*
[c] *Institute of Computer Aided Design, Russian Academy of Sciences, Moscow, 123056 Russia*
[d] *Schmidt Institute of Physics of the Earth, Russian Academy of Sciences, Moscow, 123242 Russia*
**e-mail: vmabk@cs.msu.ru*
***e-mail: chechetv@gmail.com*
****e-mail: pmsk7@mail.ru*
Received October 8, 2017

Abstract—The flow structure induced by thermal convection in a rotating spherical shell with viscous boundary conditions is considered under the assumption that the differential rotation of the core relative to the mantle is absent. The radial, azimuthal, and meridional components of the flow's velocity and helicity are studied. With the magnetic field assumed to be frozen into a liquid (frozen-flux hypothesis), it is shown that the numerical results fit the observations of the geomagnetic field variations close to the pole.

DOI: 10.1134/S1069351318030011

INTRODUCTION

The first results of three-dimensional (3D) numerical geodynamo simulations in which the generated magnetic field had a quasi-dipole structure similar to that observed on the surface of the Earth were published in 1995 (Glatzmaier and Roberts, 1995). The generation of the magnetic field in the presence of thermal convection in a rotating spherical shell filled with a conductive liquid was studied. The geometrical parameters of the shell corresponded to the Earth, whereas the classical similarity criteria, despite being significantly different from the Earth's geometrical parameters in magnitude, were selected in such a way as to reproduce a magnetic field similar to the geomagnetic field.

One of the predictions made by these calculations concerned the superrotation of the conductive inner core of the Earth due to the action of the electromagnetic torque of the geomagnetic field: the magnetic field, frozen into both a solid core and "thermal wind" (eastward flow close to the solid core), will entrain the solid core in the direction of the flow. The differential rotation of the inner core and the mantle results in the formation of the so-called tangential cylinder—a cylindrical surface with the generating lines tangential to the inner core on its equator. The axis of the cylinder coincides with the rotational axis of the shell and its radius is equal to the radius of the inner core. This cylinder is a consequence of the formation of Shercliff layers. As a result, the liquid becomes subdivided into domains above/below the inner core and the remaining part—beyond these domains. Importantly, the convection in these domains has different properties. At the onset of convection, the flows are concentrated beyond the tangent cylinder; however; at higher Reynolds numbers, the flows penetrate into the cylinder. In some models, e.g., (Glatzmayer and Roberts, 1995), a specific flow structure develops in the vicinity of the rotation axis, i.e., inside the cylinder. This structure consists of the eastward jet close to the solid core and the opposite (westward) jet near the boundary between the liquid core and the mantle. It should be noted that this structure is not always observed (Kuang and Bloxham, 1997). In the latter case, the boundary conditions were nonviscous, which probably caused the difference from the calculation of (Glatzmayer and Roberts, 1995).

It is believed that the structure of the flow close to the pole of the rotating spherical shell is determined by the thermal wind in the vicinity of the solid core, the subsequent upwelling and spreading of the flow at the boundary of the liquid core and the mantle (Olson and Aurnou, 1999; Reshetnyak and Pavlov, 2016). With the assumption of the frozen-flux hypothesis, it can be expected that due to the spreading of the conductive liquid close to the pole on the core–mantle boundary

(CMB), the radial component of the magnetic field on the Earth's surface would be reduced, and this was actually observed by Olson and Aurnou (1999). This flow structure is yet another result of the numerical simulation not previously known. We note that directly at the pole, even a weak reversed magnetic field is observed. At the same time, the role of this polar flow in the generation of the geomagnetic field is still unclear. Therefore, the generation and evolution conditions of the polar flow in the rotating spherical shell need further study.

In this work, we consider the structure of the polar flow induced by thermal convection in a rotating spherical shell with viscous boundary conditions but with the assumption that the differential rotation of the core and mantle is absent. This assumption will be substantiated in the discussion of the obtained results. The discussion also involves the questions of the generation of the geomagnertic field (geodynamo).

MATHEMATICAL MODEL

We assume that the material motion of the liquid outer core of the Earth is described by the system of equations for a viscous ideal gas (Landau and Lifshits, 1986) in the spherical coordinate system (r, φ, ψ) where the conversion to the Cartesian coordinates (x, y, z) is prescribed by the formulas $x = r\cos\varphi\cos\psi$, $y = r\sin\varphi\cos\psi$, and $z = r\sin\psi$, where $r \geq 0$, $\varphi \in [0; 2\pi)$ and $\psi \in [-\pi/2; \pi/2]$:

$$\frac{\partial \mathbf{q}}{\partial t} + \frac{\partial \mathbf{F}}{\partial r} + \frac{1}{r\cos\psi}\frac{\partial \mathbf{G}}{\partial \varphi} + \frac{1}{r}\frac{\partial \mathbf{H}}{\partial \psi} = \mathbf{R} + \mathbf{R}_\sigma + \mathbf{R}_g,$$

$$\mathbf{q} = (\rho, \rho u, \rho v, \rho w, \rho E)^T,$$

$$\mathbf{F} = (\rho u, \rho u^2 + p, \rho uv, \rho uw, \rho uH)^T,$$

$$\mathbf{G} = (\rho v, \rho vu, \rho v^2 + p, \rho vw, \rho vH)^T,$$

$$\mathbf{H} = (\rho w, \rho wu, \rho wv, \rho w^2 + p, \rho wH)^T,$$

$$\mathbf{R} = -\frac{\rho}{r}\begin{pmatrix} 2u - w\tan\psi \\ 2u^2 - v^2 - w^2 - uw\tan\psi \\ 3uv - 2vw\tan\psi \\ 3uw - (w^2 - v^2)\tan\psi \\ (2u - w\tan\psi)H \end{pmatrix}, \quad (1)$$

$$\mathbf{R}_\sigma = \begin{pmatrix} 0 \\ (\mathrm{div}\boldsymbol{\sigma})_r \\ (\mathrm{div}\boldsymbol{\sigma})_\phi \\ (\mathrm{div}\boldsymbol{\sigma})_\psi \\ \mathrm{div}(\boldsymbol{\sigma}\mathbf{v}) \end{pmatrix}, \quad p = (\gamma - 1)\rho\varepsilon, \quad E = \varepsilon + \mathbf{v}^2/2,$$

$$H = E + p/\rho, \quad \mathbf{v} = (u, v, w).$$

Here, t is time, ρ is gas density, p is pressure, ε is specific (mass) internal energy, E is total specific energy, H is total specific enthalpy, $\mathbf{v}$ is velocity of gas with the components (u, v, w) in the local orthonormal basis of the spherical coordinates $(\mathbf{e}_r, \mathbf{e}_\varphi, \mathbf{e}_\psi)$, γ is the adiabatic exponent, $\boldsymbol{\sigma}$ is the iscous stress tensor, and $\mathbf{R}_g$ is the specific (volumetric) gravity force.

The components of the viscous stress tensor $\boldsymbol{\sigma}$ in the spherical coordinates have the following form (Kochin, 1965):

$$\sigma_{rr} = (2\mu + \lambda)\frac{\partial u}{\partial r} + \frac{\lambda}{r\cos\psi}\frac{\partial v}{\partial \varphi} + \frac{\lambda}{r}\left(\frac{\partial w}{\partial \psi} + 2u - w\tan\psi\right),$$

$$\sigma_{\varphi\varphi} = \lambda\frac{\partial u}{\partial r} + \frac{2\mu + \lambda}{r}\left(\frac{1}{\cos\psi}\frac{\partial v}{\partial \varphi} - w\tan\psi\right) + \frac{\lambda}{r}\frac{\partial w}{\partial \psi} + (\mu + \lambda)\frac{2u}{r},$$

$$\sigma_{\psi\psi} = \lambda\frac{\partial u}{\partial r} + \frac{\lambda}{r\cos\psi}\frac{\partial v}{\partial \varphi} + \frac{2\mu + \lambda}{r}\frac{\partial w}{\partial \psi} + (\mu + \lambda)\frac{2u}{r} - \frac{\lambda}{r}w\tan\psi,$$

$$\sigma_{r\varphi} = \sigma_{\varphi r} = \mu\left(\frac{\partial v}{\partial r} + \frac{1}{r\cos\psi}\frac{\partial u}{\partial \varphi} - \frac{v}{r}\right),$$

$$\sigma_{r\psi} = \sigma_{\psi r} = \mu\left(\frac{\partial w}{\partial r} + \frac{1}{r}\frac{\partial u}{\partial \psi} - \frac{w}{r}\right),$$

$$\sigma_{\varphi\psi} = \sigma_{\psi\varphi} = \mu\left(\frac{1}{r\cos\psi}\frac{\partial w}{\partial \varphi} + \frac{1}{r}\frac{\partial v}{\partial \psi} + \frac{v}{r}\tan\psi\right).$$

Here, $\mu = \nu\rho$ is the coefficient of dynamic viscosity, ν is the coefficient of kinematic viscosity, and $\lambda = \zeta - 2\mu/3$, where ζ is the coefficient of the second viscosity, hereinafter, assumed to be zero. The components of vector $\mathbf{R}_\sigma$ in the system of Eqs. (1) can be written out in the following form:

$$(\mathrm{div}\,\boldsymbol{\sigma})_r = \frac{\partial \sigma_{rr}}{\partial r} + \frac{1}{r\cos\psi}\frac{\partial \sigma_{\varphi r}}{\partial \varphi} + \frac{1}{r}\frac{\partial \sigma_{\psi r}}{\partial \psi} + \frac{2\sigma_{rr} - \sigma_{\varphi\varphi} - \sigma_{\psi\psi} - \sigma_{\psi r}\tan\psi}{r},$$

$$(\mathrm{div}\,\boldsymbol{\sigma})_\varphi = \frac{\partial \sigma_{r\varphi}}{\partial r} + \frac{1}{r\cos\psi}\frac{\partial \sigma_{\varphi\varphi}}{\partial \varphi} + \frac{1}{r}\frac{\partial \sigma_{\psi\varphi}}{\partial \psi} + \frac{3\sigma_{r\varphi} - 2\sigma_{\psi\varphi}\tan\psi}{r},$$

$$(\mathrm{div}\,\boldsymbol{\sigma})_\psi = \frac{\partial \sigma_{r\psi}}{\partial r} + \frac{1}{r\cos\psi}\frac{\partial \sigma_{\varphi\psi}}{\partial \varphi} + \frac{1}{r}\frac{\partial \sigma_{\psi\psi}}{\partial \psi} + \frac{3\sigma_{r\psi} + (\sigma_{\varphi\varphi} - \sigma_{\psi\psi})\tan\psi}{r},$$

$$\mathrm{div}(\boldsymbol{\sigma}\mathbf{v}) = \frac{1}{r^2}\frac{\partial}{\partial r}\left(r^2\left(u\sigma_{rr} + v\sigma_{r\phi} + w\sigma_{r\psi}\right)\right) + \frac{1}{r\cos\psi}\frac{\partial}{\partial \varphi}\left(u\sigma_{\varphi r} + v\sigma_{\varphi\varphi} + w\sigma_{\varphi\psi}\right)$$

$$+\frac{1}{r\cos\psi}\frac{\partial}{\partial\psi}\left(\cos\psi\left(u\sigma_{\psi r}+v\sigma_{\psi\varphi}+w\sigma_{\psi\psi}\right)\right).$$

Let us find the stationary cylindrically symmetric solution of system (1). We assume that

$$\frac{\partial\cdot}{\partial t}=0,\quad \frac{\partial\cdot}{\partial\varphi}=0,\quad u=w=0 \text{ and}$$
$$v(r,\psi)=\omega r\cos\psi.$$

Here, ω is the constant angular velocity of gas rotation. We note that with the adopted assumptions $\operatorname{div}\boldsymbol{\sigma}=0$ and $\operatorname{div}(\boldsymbol{\sigma}\mathbf{v})=0$ (at $\mu=\text{const}$). We also assume that the free-fall acceleration g is directed towards the center of the spherical coordinate system; then, $\mathbf{R}_g=(0,\rho g,0,0,0)^T$ and $g=g(r)$; i.e., it is only radius dependent, where the given function $g(r)$ has the antiderivative $G(r)$. Under these assumptions, the system of equations (1) takes on the following form:

$$\frac{\partial p}{\partial r}=\frac{\rho v^2}{r}-\rho g,\quad \frac{1}{r}\frac{\partial p}{\partial\psi}=-\frac{\rho v^2}{r}\tan\psi.$$

Let us find the solution of these equations assuming power-law pressure dependence on density $p=\kappa\rho^\alpha$, $\kappa,\alpha=\text{const}$, and $\alpha\neq 1$. Finding this solution is reduced to integrating the system of equations

$$\kappa\alpha\rho^{\alpha-2}\frac{\partial\rho}{\partial r}=\omega^2 r\cos^2\psi-g,$$
$$\kappa\alpha\rho^{\alpha-2}\frac{\partial\rho}{\partial\psi}=-\omega^2 r^2\sin\psi\cos\psi.$$

From the second equation,

$$\frac{\kappa\alpha}{\alpha-1}\rho^{\alpha-1}=\frac{\omega^2}{2}r^2\cos^2\psi+c(r),$$

where $c(r)$ is the arbitrary function of variable r. Hence, considering the first equation, we obtain

$$\kappa\alpha\rho^{\alpha-2}\frac{\partial\rho}{\partial r}=\omega^2 r\cos^2\psi+c'(r)$$
$$=\omega^2 r\cos^2\psi-g\Rightarrow c(r)=\bar{c}-G(r).$$

As a result, we come to the following equilibrium distribution of gas parameters, which will hereinafter be used as the initial data in the problem concerned:

$$\rho=\left[\frac{\alpha-1}{\kappa\alpha}\left(\bar{c}+\frac{v^2}{2}-G(r)\right)\right]^{\frac{1}{\alpha-1}},\quad p=\kappa\rho^\alpha,$$
$$v=\omega r\cos\psi,\quad u=w=0,\quad \kappa=\frac{\bar{p}}{\bar{\rho}^\alpha},\qquad (2)$$
$$\bar{c}=\frac{\alpha\bar{p}}{(\alpha-1)\bar{\rho}}+G(\bar{r}).$$

Here, it is assumed that at some $r=\bar{r}$ and $\psi=\pm\pi/2$, the pressure and density values are known ($\bar{p}$ and $\bar{\rho}$, respectively).

We note that the value $\alpha=1$ corresponds to the constant distribution of temperature T with a spatially stationary configuration. Then, from the equation of state $p=\rho RT$ where R is the gas constant, we obtain the linear density dependence for pressure $p=\kappa\rho$ and $\kappa=RT=\text{const}$. In this case, in a similar way, we obtain the following equilibrium density distribution:

$$\rho(r,\psi)=\bar{\rho}\exp\left\{\frac{1}{\kappa}\left(\frac{\omega^2}{2}r^2\cos^2\psi-G(r)\right)\right\},$$
$$\bar{\rho}=\text{const}.$$

Currently there are different models describing the structure of the Earth. At the same time, only a few parameters of the Earth are known, in particular, the radius $r_E\approx 6.371\times10^6$ m and angular velocity $\omega_E\approx 7.292\times10^{-5}\ \text{s}^{-1}$. It is believed that the liquid core occupies the domain $r\in[r_1,r_2]$ where $r_1\approx 1.3\times10^6$ m and $r_2\approx 3.5\times10^6$ m. The material parameters of the liquid core at these distances from the center are approximately determined with the use of various models and experiments. In particular, temperature, pressure, and density are estimated at

$$T_1\approx 6\times10^3\ \text{K},\quad T_2\approx 4.3\times10^3\ \text{K};$$
$$p_1\approx 3\times10^{11}\ \text{Pa},\quad p_2\approx 1.3\times10^{11}\ \text{Pa};$$
$$\rho_1\approx 1.2\times10^4\ \text{kg}/\text{m}^3,\quad \rho_2\approx 0.55\times10^4\ \text{kg}/\text{m}^3 \qquad (3)$$
$$(\text{up to } 9.9\times10^4).$$

The free-fall acceleration at the external boundary of the liquid core is estimated at $g_2=10.4\ \text{m/s}^2$ and decreases to zero towards the center of the Earth with a decay pattern assumed to be linear. Hence, $g(r)=g_2 r/r_2$ and $G(r)=g_2 r^2/(2r_2)$.

In order for the equilibrium distribution (2) to approximately fit values (3), we selected the following parameters: $\bar{r}=r_2$, $\bar{\rho}=\rho_2$, $\bar{p}=p_2$, and $\alpha=5/3$. The gas constant was specified by $R=3800\ \text{m}^2/\text{s}^2\ \text{K}$.

The calculations described below were conducted in the mobile coordinate system rotating at a constant angular velocity $\omega=\omega_E$ around the axis $\psi=\pm\pi/2$. In this case, the right-hand side of Eqs. (1) additionally contains the noninertial centrifugal and Coriolis forces:

$$\mathbf{R}_\omega=(\mathbf{R}_\omega^{(1)},\mathbf{R}_\omega^{(2)},\mathbf{R}_\omega^{(3)},\mathbf{R}_\omega^{(4)},\mathbf{R}_\omega^{(5)})^T,\quad \mathbf{R}_\omega^{(1)}=0,$$
$$\mathbf{R}_\omega^{(2)}=\rho(\omega^2 r\cos\psi+2\omega v)\cos\psi,$$
$$\mathbf{R}_\omega^{(3)}=2\rho\omega(w\sin\psi-u\cos\psi),$$
$$\mathbf{R}_\omega^{(4)}=-\rho(\omega^2 r\cos\psi+2\omega v)\sin\psi,$$
$$\mathbf{R}_\omega^{(5)}=u\mathbf{R}_\omega^{(2)}+v\mathbf{R}_\omega^{(3)}+w\mathbf{R}_\omega^{(4)}.$$

For the subsequent analysis, it is convenient to make the problem dimensionless. To do this, we select the following scaling factors:

$$r_0 = 10^6 \text{ m}, \quad T_0 = 5\times10^3 \text{ K},$$
$$\rho_0 = 10^4 \text{ kg}/\text{m}^3, \quad p_0 = 10^{11} \text{ Pa}.$$

We introduce the dimensionless variables, hereinafter, marked by a prime sign, according to the following formulas:

$$t = t_0 t', \quad r = r_0 r', \quad \mathbf{v} = v_0 \mathbf{v}', \quad \omega = \omega_0 \omega',$$
$$g = g_0 g', \quad p = p_0 p', \quad \rho = \rho_0 \rho',$$
$$T = T_0 T', \quad R = R_0 R'.$$

Let us express coefficients t_0, v_0, ω_0, g_0, and R_0 in terms of the selected scaling factors:

$$t_0 = r_0\sqrt{\frac{\rho_0}{p_0}}, \quad v_0 = \sqrt{\frac{p_0}{\rho_0}},$$
$$\omega_0 = \frac{1}{r_0}\sqrt{\frac{p_0}{\rho_0}}, \quad g_0 = \frac{p_0}{r_0\rho_0}, \quad R_0 = \frac{p_0}{T_0\rho_0}.$$

Then, system (1) in the dimensionless variables preserves its original form. Hereinafter, only these variables are used and the prime mark in their designations is omitted.

NUMERICAL RESULTS

The calculations described below are based on the explicit conservative Godunov-type difference scheme (Godunov, 1959; Godunov and Zabrodin, 1961) in which the grid flows of the first-order approximation were calculated by Roe's method (Roe, 1986) with Einfeld's modifications (Einfeld, 1988) to avoid nonphysical breaks in the numerical solution. Osher's grid flow correction (Chakravarthy and Osher, 1985) implemented in the computations raised the approximation order of the scheme to 3. The technique for adapting this scheme for the case of spherical coordinates and for allowing for the viscous stress tensor is described in detail in (Abakumov, 2015).

The calculations were conducted within a bounded domain of the spherical coordinates $r_1 \le r \le r_2$, with $r_1 = 1.3$ and $r_2 = 3.5$. At the domain boundary, no-slip conditions were imposed: $\mathbf{v}(r_1, \varphi, \psi) = 0$, $\mathbf{v}(r_2, \varphi, \psi) = 0$ (in a rotating coordinate system). The initial data were specified by the equilibrium configuration with the parameters described in the previous section. The kinematic viscosity ν was set to be constant and its dimensionless value in the different variants of the calculations varied from 2×10^{-4} to 1×10^{-2}. With the different viscosity values from this range, no significant distinctions appeared in the numerical results. Both the two-dimensional (2D) and three-dimensional (3D) calculations were carried out. In the 2D cases, the calculations were conducted in one layer of the difference cells with a fixed polar angle and assumed cylindrical symmetry of the flow. The three velocity components were calculated and a 3D grid was used. We note that in the course of simulations, the 3D calculations did not differ from their 2D counterparts; i.e., a heterogeneity of the flow in terms of the polar angle did not develop. This allowed us to manage with a 2D approximation for most variants of the numerical simulation.

Let us now focus on the characteristic numerical results. At the initial modeling stage, the starting equilibrium configuration does not undergo any significant changes. The velocity components do not noticeably deviate from zero. However, the situation changes by the time $T \approx 400$. Here, the vortices arise close to the inner boundary of the calculation domain, which is reflected in the emergence of heterogeneities in all the velocity components. Note that the dimensionless time unit is about 316 s and $T = 273$ approximately corresponds to one day.

Figure 1 shows the lines of the component values and the vectors of gas velocity for the time $T = 540$. The diagrams clearly demonstrate the characteristic jets directed from the inner boundary of the calculation domain to its periphery. The presence of the vortex motion can be inferred from the existence of the adjacent regions having opposite signs of the meridional velocity component.

The emergence of the jets is concomitant with the deviation of the gas rotation velocity from the initially constant value. These deviations are most significant in the vicinity of the rotation axis. Here, the rotation of the gas speeds up close to the inner boundary and slows down close to the outer boundary (Fig. 1).

It is worth noting that the jets do not reach the outer boundary of the domain: they almost completely lose their intensity after passing about 2/3 of the distance between the boundaries. A weak backflow takes place, and, due to the viscosity, the flow tends to regain its undisturbed state. However, the new vortices emerge close to the boundary, and the process recurs on a quasi-periodic basis (Fig. 2, $T = 990$).

We note that although the symmetrical jets commence near different segments of the inner boundary, their intensity is highest in the vicinity of the rotation axis (Fig. 2). With the emergence of the jets, the flow helicity ($\mathbf{v} \cdot \text{curl}\mathbf{v}$) in the respective regions becomes nonzero. The lines of the helicity values for time $T = 540$ and $T = 990$ are shown in Fig. 3. It can be seen that the helicity is higher at the higher intensity of the jets.

Concluding this point we note that the described quasi-periodic character of the flow was preserved during the entire calculation time $T = 4000$.

DISCUSSION AND CONCLUSIONS

Let us briefly summarize the results yielded by the numerical simulation of a rotating spherical shell with

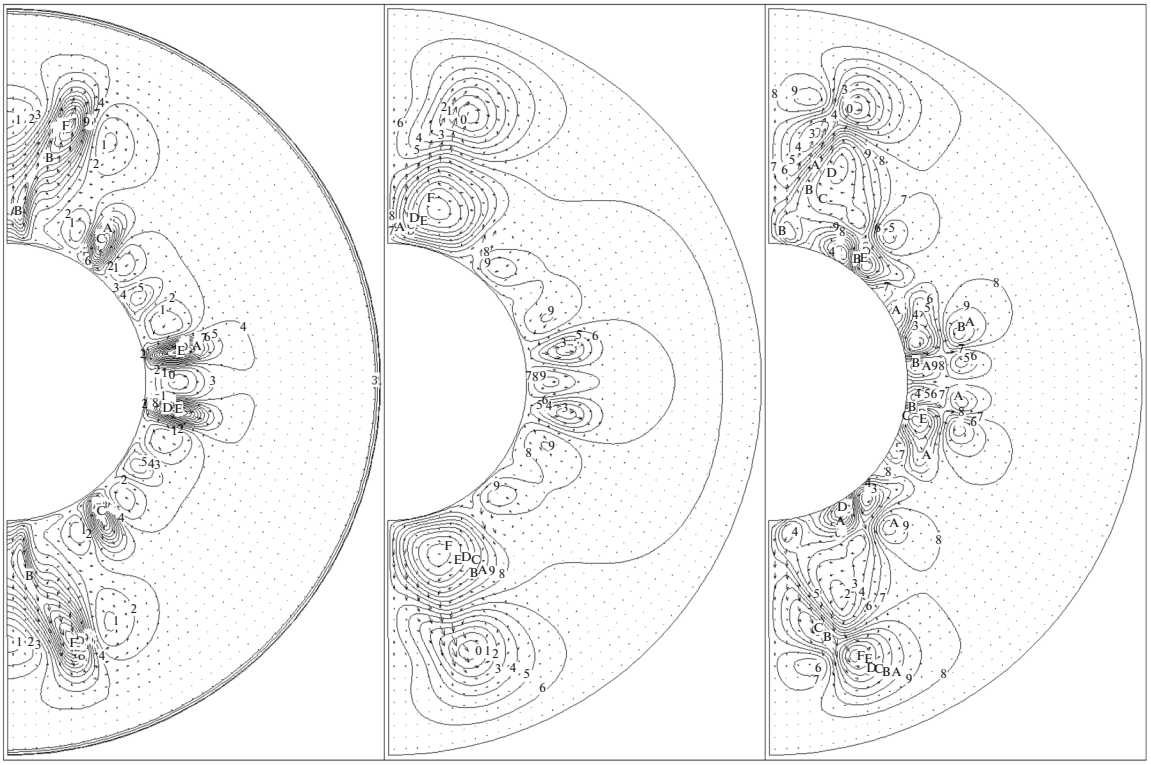

Fig. 1. Velocity components at $T = 540$. From left to right: radial, azimuthal, meridional.

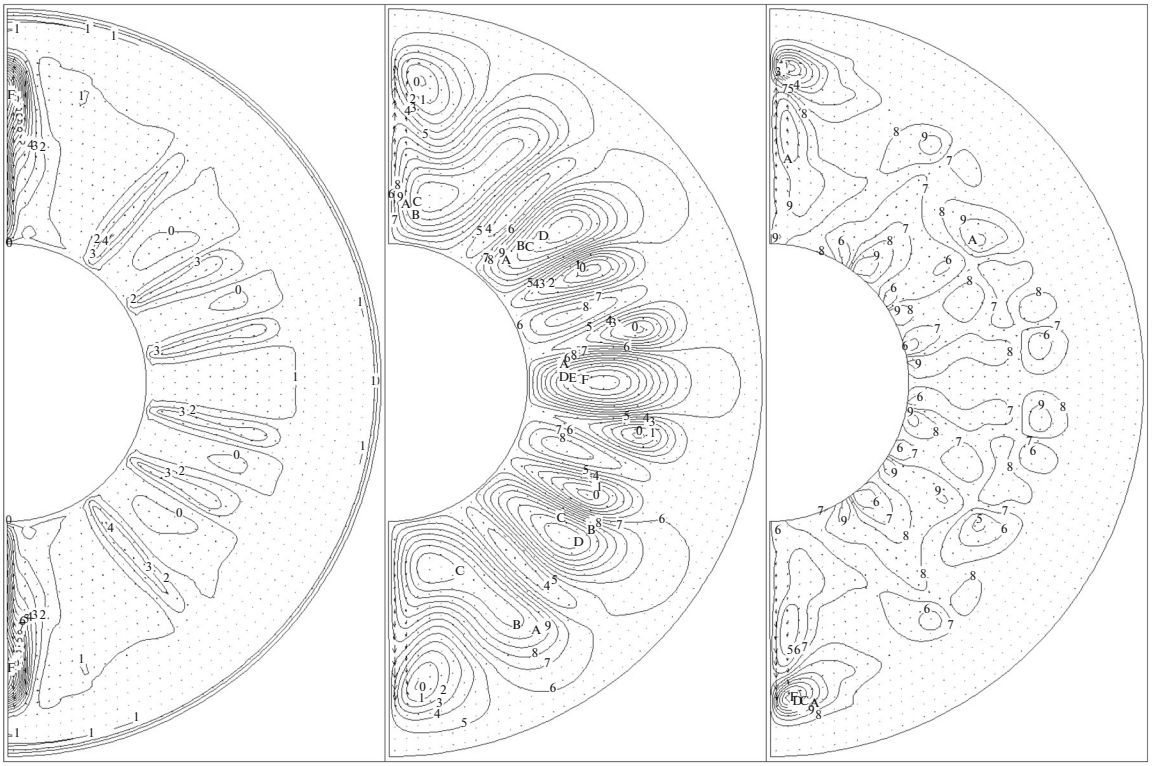

Fig. 2. Velocity components at $T = 990$. From left to right: radial, azimuthal, meridional.

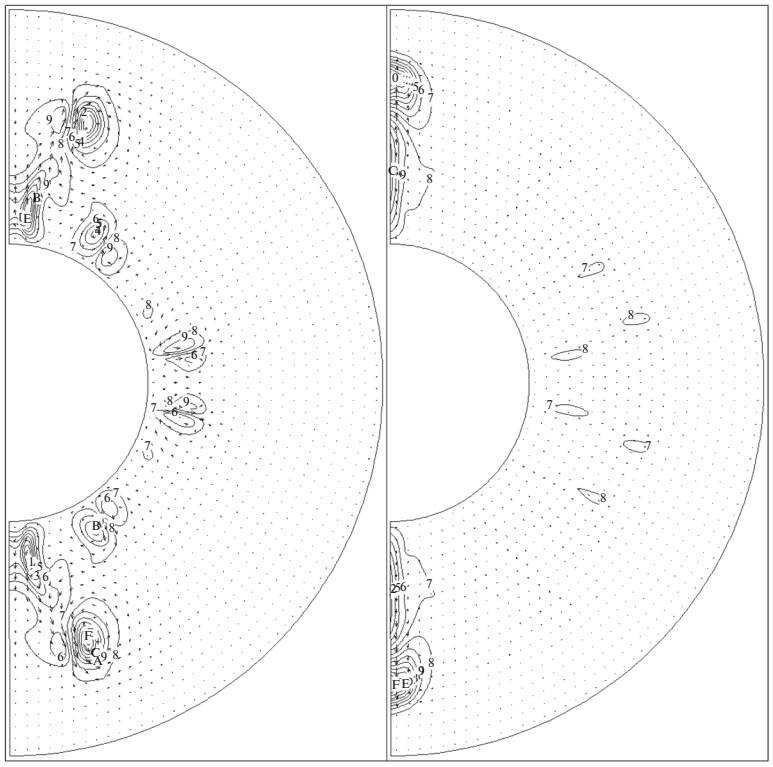

Fig. 3. Helicity at $T = 540$ (left) and $T = 990$ (right).

the main focus placed on the vicinity of the rotation axis.

(1) The radial component of the fluid velocity in the vicinity of the rotation axis shows a large-scale upwelling motion slightly deviating from the axis, whereas on the rotation axis itself, a backflow (towards the inner shell) is predominant. After the flow pattern collapses, the structure tends to get restored, and the upwelling along the rotation is predominant; however, with the lapse of time, the upwelling fades and a weak backflow appears in the vicinity of the axis. (We note that quasi-periodicity in the recurrence of the flow pattern was observed in all the velocity components and had not been noted previously).

(2) The azimuthal component of the fluid velocity corresponds to the structure of the flow where, in the vicinity of the inner shell, the velocity is directed eastwards, whereas at the boundary between the outer shell and the liquid (close to the projection of the inner sphere onto the outer sphere), the velocity is directed westwards. Thos flow pattern is also unstable, and after collapsing it tends to recover. Here, at the latitudes higher than the projection of the inner sphere onto the outer sphere, the east–west jets alternately emerge and disappear. The pattern generally resembles torsional oscillations in the polar latitudes.

(3) The meridional component of the flow velocity under a mature upwelling is directed from the rotation axis in the vicinity of the boundary between the liquid and the outer shell. This flow pattern overall can be again reproduced after collapsing; however, the smaller scale features appear.

Let us see now, how the numerical results could fit the processes in the liquid core of the Earth.

The differential rotation of the Earth's solid core and the mantle has been initially identified based on the 30-year time series of the travel time data for the seismic *P*-waves passing through the inner core (Song and Richards, 1996). It was concluded that the core rotates 1° per annum faster than the mantle. In (Vidale and Earle, 2000) the latter value was reduced to ~0.16° per annum. The broad scatter in the estimates of the differential rotation can be caused by the sensitivity of the body waves to local heterogeneities in the structure of the inner core (Laske and Masters, 1999). Therefore, the authors of the last work proposed an alternative method using the large-scale split modes of the free oscillations of the Earth which, in contrast to the short-period seismic oscillations, are independent of the position of the radiation source and insensitive to small-scale heterogeneities. Based on the data for a 20-year period, we estimated the average difference $\Delta\Omega = 0.01° \pm 0.21°$/yr, which probably constrains the maximal value of $\Delta\Omega$ so that $\Delta\Omega \le 0.2°–0.3°$. If, following (Laske and Masters, 1999), we only take into account the superrotation of the core, we obtain the constraint $\Delta\Omega = (0.01–0.3)°$/yr or $\Delta\Omega = (0.06–1.8)\times10^{-10}$ s^{-1} (which testifies to the fairly

high viscosity of the inner core (Shalimov, 2005)). Taking into account the scatter in the determination of $\Delta\Omega$ suggests the conclusion about the absence of the rotation of the core relative to the mantle (Laske and Masters, 1999). Following this conclusion, we assumed the absence of the rotation of the core relative to the mantle in the calculations in the present work.

As was noted in the introduction, assuming the frozen-flux hypothesis, we may expect the reduction in the radial component of the magnetic field on the Earth's surface due to the spreading of the conductive liquid close to the pole at the core–mantle boundary. In this case, a weak field of the reversed polarity is observed directly at the pole. The numerical results (point (1), the flow structure reflected in the radial component of the velocity) are fairly consistent with the observations.

As is known, vast magnetic anomalies, which reflect the state of the magnetic field on the surface of the liquid core, i.e., at the core–mantle boundary, are observed on the Earth's surface. This refers to patches of a high-intensity magnetic field (four patches overall), approximately symmetric about the equator and centered at the intersection of the parallels (60° N and 60° S) and meridians (120° E and 120° W, respectively). In the northern hemisphere, these patches are centered in Siberia and North America. These anomalies were detected for the first time by processing the historical observations (Bloxham and Gubbins, 1987; Johnson et al., 2003) and subsequently validated and refined by the observations of the satellite missions Magsat 1980 and Oersted 2000 (Hulot et al., 2002). With the assumption that the geomagnetic field lines are frozen into a liquid, the observations suggest the following conclusion: the flow on the surface of the liquid core is a system of four large-scale vortices. It turned out that these vortices are drifting westwards (Olson and Aurnou, 1999), and this conclusion was supported by the later high-resolution satellite observations (Hulot et al., 2002). The latest conclusion inferred from the Swarm satellite data for 2000–2016 (Livermore et al., 2016) indicates the presence of a nonaxisymmetric large-scale westward jet close to the projection of the tangent cylinder onto the Earth' surface, and this jet includes and accelerates the mentioned vortices. Interestingly, Libvermore et al. (2016) consider it possible that, firstly, the jet may change its direction and, secondly, the jet serves as a source of torsional oscillations in the liquid core.

Hence, the results of the model calculations are soundly supported by the observations of the magnetic field close to the pole (point 2).

Let us consider the probable role of the azimuthal velocity shear (along the altitude) in the generation of the geomagnetic field. In the presence of the dipole component of the poloidal magnetic field, the shear flow will lead to the Ω-effect—a strong axisymmetric toroidal component within the imaginary tangential cylinder. It can be expected that close to the core the azimuthal field will partially suppress the turbulent convection. Therefore the turbulence area will be concentrated close to the liquid core–mantle boundary and will be a source of helical waves (inertial or magnetostrophic). The propagation of these waves through the area of the azimuthal field may lead to the α-effect—generation of the poloidal component of the field from the azimuthal component. Hence, the α-Ω geodynamo mechanism capable of maintaining the dipole component of the geomagnetic field is probable. We note that using the frozen-flux hypothesis in the analysis of the α effect is, strictly speaking, illegitimate. The corresponding magnetohydrodynamic calculation will be presented in a future work.

ACKNOWLEDGMENTS

We pay tribute to the late Yury P. Popov, corresponding member of the Russian Academy of Sciences. He helped start our work and determined its concept. Our deep gratitude goes to his valuable comments and suggestions. In blessed memory of him.

The work was supported by the Russian Science Foundation (project no. 16–11-10339).

REFERENCES

Abakumov, M.V., Construction of Godunov-type difference schemes in curvilinear coordinates and an application to spherical coordinates, *Comput. Math. Model.*, 2015, vol. 26, no. 2, pp. 184–203.

Bloxham, J. and Gubbins, D., Thermal core-mantle interactions, *Nature*, 1987, vol. 325, pp. 511–513.

Chakravarthy, S.R. and Osher, S., A new class of high accuracy TVD schemes for hyperbolic conservation laws, American Institute of Aeronautics and Astronautics (AIAA) Paper 85-0363, *AIAA Meeting Papers, 23rd Aerospace Science Meeting* (Reno, Nevada, 1985), 1985, pp. 1–11.

Einfeldt, B., On Godunov-type methods for gas dynamics, *Soc. Ind. Appl. Math. (SIAM) J. Numer. Anal.*, 1988, vol. 25, no. 2, pp. 294–318.

Glatzmaier, G.A. and Roberts, P.H., A three-dimensional self-consistent computer simulation of a geomagnetic field reversal, *Nature*, 1995, vol. 337, pp. 203–209.

Godunov, S.K., Difference method for numerical calculation of discontinuous solutions of fluid dynamics, *Mat. Sb.*, 1959, vol. 47 (89), no. 3, pp. 271–306.

Godunov, S.K., Zabrodin, A.V., and Prokopov, G.P., A difference scheme for two-dimensional nonstationary problems of gas dynamics and flow calculation with a detached shock wave, *Zh. Vychisl. Mat. Mat. Fiz.*, 1961, vol. 1, no. 6, pp. 1020–1050.

Hulot, G., Eymin, C., Langlais, B., Mandea, M., and Olsen, N., Small-scale structure of the geodynamo inferred from Oersted and Magsat satellite data, *Nature*, 2002, vol. 416, no. 6881, pp. 620–623.

Johnson, C.L., Constable, C.G., and Tauxe, L., Mapping longterm changes in Earth's magnetic field, *Science*, 2003, vol. 300, pp. 2044–2045.

Kochin, N.E., *Vektornoe ischislenie i nachala tenzornogo ischisleniya* (Vector Calculus and Basics of Tensor Calculus), Moscow: Nauka, 1965.

Landau, L.D. and Lifshits, E.M., *Teoreticheskaya fizika. T. 6. Gidrodinamika*. (Theoretical Physics, vol. 6: Fluid Mechanics) Moscow: Nauka, 1986.

Laske, G. and Masters, G., Rotation of the inner core from a new analysis of free oscillations, *Nature*, 1999, vol. 402, pp. 66–69.

Livermore, P.W., Hollerbach, R., and Finlay, C.C., An accelerating high-latitude jet in Earth's core, *Nat. Geosci*., 2016. doi 10.1038/NGEO2859

Olson, P. and Aurnou, J., A polar vortex in the Earth's core, *Nature*, 1999, vol. 402, pp. 170–173.

Reshetnyak, M.Yu. and Pavlov, V.E., Evolution of the dipole geomagnetic field. Observations and models, *Geomagn. Aeron*., 2016, vol. 56, no. 1, pp. 110–124.

Roe, P.L., Characteristic-based schemes for the Euler equations, *Ann. Rev. Fluid Mech*., 1986, vol. 18, pp. 337–365.

Shalimov, S.L., Estimation of the Earth's outer core ductility based on differential rotation of the mantle and the inner core, *Geofiz. Issled*., 2005, no. 2, pp. 129–132.

Song, X. and Richards, P.G., Seismological evidence for differential rotation of the Earth's inner core, *Nature*, 1996, vol. 382, pp. 221–224.

Vidale, J.E. and Earle, P.S., Fine-scale heterogeneity in the Earth's inner core, *Nature*, 2000, vol. 404, pp. 273–275.

Translated by M. Nazarenko